Organic Sensors

Zitierweise:
Internationale Ausgabe: doi.org/10.1002/anie.202203358
Deutsche Ausgabe: doi.org/10.1002/ange.202203358

Electronic Tuning in Reaction-Based Fluorescent Sensing for Instantaneous and Ultrasensitive Visualization of Ethylenediamine

Yulei Ke[+], Yuan Liu[+], Baiyi Zu, Da Lei, Guangfa Wang, Jiguang Li, Wenfei Ren, and Xincun Dou**

Abstract: Manipulation of a multi-physical quantity to steer a molecular photophysical property is of great significance in improving sensing performance. Here, an investigation on how a physical quantity rooted in the molecular structure induces an optical behavior change to facilitate ultrasensitive detection of ethylenediamine (EDA) is performed by varying a set of thiols. The model molecule consisting of a thiol with dual-carboxyl exhibits the strongest fluorescence, which is ascribed to the electron-donating ability and prompted larger orbital overlap and oscillator strength. The elevated fluorescence positively corelated to the increased EDA, endowing an ultrasensitive response to the nanomolar-liquid/ppm-vapor. A gas detector with superior performance fulfills a contactless and real-time management of EDA. We envisage this electron-tuning strategy-enabled fluorescence enhancement can offer in-depth insight in advancing molecule-customized design, further paving the way to widening applications.

Introduction

Sensitive and rapid on-site probing of toxic and hazardous substances is of great significance as it can effectively stem severe threats to public security and health arising from industrial leakage or explosive-related terrorist attacks.[1] Either considering the crucial roles in industry or explosive manufacture by terrorists (e.g., Picatinny liquid explosive), ethylenediamine (1,2-diamines, EDA) has forced our society to take its presence seriously.[2] Its highly corrosive and toxic properties easily places human beings and creatures including aquatic animals in danger on exposure to vaporous EDA at a low concentration, for example, 10 ppm EDA was specified by the WHO as an occupational exposure limit.[3] The severe risk, such as acute kidney injury and tumorigenesis, can be triggered by simple skin contact and inhalation of EDA. Therefore, there is a pressing demand for on-site detection of EDA with a high sensitivity, rapid response, and real-time monitoring to prevent its potential threat to human health, public security, and environmental sustainability. Growing attention has been dedicated to developing EDA determination methodologies based on gas chromatography–mass spectrometry,[4] high performance liquid chromatography,[5] electrochemistry,[6] colorimetry,[7] and fluorescence spectroscopy,[8] etc. On account of the features including fast response, ease of operation and visualization, a fluorescence probe is deemed to fit more and has been adapted for the on-site application.[9] However, the response time and sensitivity of the reported fluorescence methods still needs to be improved to meet the requirement in real applications.[8,10] Generally, a fluorescence probe comprising a fluorophore as the main skeleton and other chemical groups as specific binding sites holds significant values owing to the diverse and controllable structure.[11] In other words, the skeleton structure substituted with varied chemical groups exhibits different photochemical properties in widening applications, such as in-field analysis.[12] It was found that the imidazole derivatives could bear the appreciable changes observed in fluorescence upon metal-ion binding via chelation, such as the sensitive interaction of imidazole-tetraphenyleghylene towards "priority pollutants" listed by the U.S. Environmental Protection Agency.[13] From the perspective of the alteration either in intensity or wavelength brought about by the interaction between the fluorogenic molecule and other substances, the mechanisms underpinned by charge transfer are more predominant because of abundant choices for constructing chemical groups to allow electron movement along the conjugation structure, leading to an impact on the potential energy surface and electron–hole separation.[14] A convincing example in this field is that the electron transferring direction as well as the conjugation extent could alter the molecular potential energy surface of both ground and excited state, respectively, inducing an excitation/emission wavelength shift.[15] Therefore, it can be reasonably inferred that the effective electron tuning prompted a molecular configuration alteration which changes the potential energy surface as evidenced by the luminescent behavior.

More fundamentally, such kinds of molecular changes are rooted in a series of physical characteristics including the

[*] Y. Ke,[+] Dr. Y. Liu,[+] Prof. B. Zu, Dr. D. Lei, Dr. G. Wang, J. Li, W. Ren, Prof. X. Dou
Xinjiang Key laboratory of Explosives Safety Science,
Xinjiang Technical Institute of Physics & Chemistry,
Chinese Academy of Sciences
Urumqi 830000 (China)
E-mail: byzu@ms.xjb.ac.cn
xcdou@ms.xjb.ac.cn

Y. Ke,[+] J. Li, W. Ren, Prof. X. Dou
Center of Materials Science and Optoelectronics Engineering,
University of Chinese Academy of Sciences
Beijing 100049 (China)

[+] These authors contributed equally to this work.

highest occupied molecular orbital (HOMO)/the lowest unoccupied molecular orbital (LUMO),[16] molecular polarity index (MPI),[17] electrostatic potential (ESP)[18] and oscillator strength (OS).[19] It has been reported that the HOMO–LUMO gap of benzene is prohibitively large, while the introduction of appropriate electronic controller groups, the frontier molecular orbitals of the parent benzene can be modulated to bring the excitation and emission energy windows to the visible wavelength range.[20] In addition, the ESP was adopted to computationally evaluate how the electron-donating moiety with different substituted positions from the electron-accepting moiety affected the thermally activated delayed fluorescence quantum efficiency and lifetime of the emitter.[21] Clearly, the fine modulation of the basic physical descriptor is an efficient pathway to seek out the most essential factor for determining the optical behaviors. Moreover, comparing with the partial consideration of one or two of the above physical quantities, an investigation of the integral outcome involving multiple quantities is required. For instance, there remains an uncertainty in wavelength-relevant factors, whether the HOMO/LUMO gap, electron-transfer and MPI all have a superposition effect to make it shift towards a spectral direction, and which factor plays a decisive role, or whether one of them contributes a negative effect. Hence, it is crucial to build a systematic model to ascertain the decisive descriptor and/or an internal relevance, accelerating the customizable molecule design, consequently tuning the fluorescence characteristics to further advance chemosensor fabrication and propel the development of luminescent material as well as devices. Whereas, thus far, the previous works do not thoroughly screen the overall influence from multi characteristics, nor do they mention the intrinsic linkage between quantities and the influence of each quantity on the fluorescence behavior. Furthermore, rare studies broke through the phase of computational discussion to experimentally demonstrate the deduction and present systems capable of coping with the realistic demand in hazardous chemicals monitoring.

Herein, from the aspect of the fluorescence generation mechanism, we targeted a fundamental descriptor—electron transferring capability to investigate how electron tuning acts on the entire molecule behavior to achieve an improved fluorescence emission in responding to EDA, a molecule model was constructed comprising a thiol-substituted heteroaromatic compound. The individual influence of the HOMO/LUMO gap, MPI, ESP and OS, as well as the multiple influence of the above relevant quantities were comprehensively analyzed when varied thiols were used in the model molecule. The strongest fluorescent emission was yielded using the thiol with the strongest electron-donating capability which restricts molecular distortion to preferentially obtain a conjugated plane. Furthermore, the optimal sensing reagent contributed a visualized response towards concentration-dependent EDA with ultra-sensitivity as well as low cross-activity toward potential co-existing substances. Moreover, a portable detector with a one-button scheme was initiated and showed great practicability and reliability.

Results and Discussion

Quantum Chemistry Computing Studies for the Influence of Physical Quantities on the Thiol-Substituted Compounds

Generally, partial chemical groups could have significant impact on the conjugation extent, electron distribution as well as the photophysical properties of the entire molecule. Here, a facile reaction between *o*-phthalaldehyde (OPTA), EDA and different thiols was employed and the product was treated as the model molecule for investigating how the thiol structure impacts on the imidazo isoindole triatomic ring named as "1" (Figure 1a).[22] Thiol with tunable electron transferring capability was chosen to carry a series of other chemical groups to provide the incremental electronegativity to the imidazo isoindole triatomic ring. An increased electronegativity was designed via linking -SH with alkene chain (allyl mercaptan, AM), hydroxy (mercaptoethanol, ME) and carboxyl (3-mercaptopropionic acid, MPA), while -SH in mercaptosuccinic acid (MSA) was connected with two carboxyls, endowing a stronger electronegativity than MPA. Four thiols were separately applied to cooperate with OPTA to react with EDA, the product (named as "1-thiol") displayed an enhanced fluorescence at 525 nm with an order of **1-MSA** > **1-MPA** > **1-ME** > **1-AM** under the optimized conditions (Figures 1b, S1). Generally, the magnitude of the electronegativity of functional groups greatly impacts on the bond length, vibration frequency, electron transfer and excited state energy, further altering the fluorescent behaviors including Stokes shift, quantum yield and lifetime.[23] Starting with the molecular essence of the above four thiol-embedded models (**1-MSA**, **1-MPA**, **1-ME** and **1-AM**), the physical properties were theoretically analyzed (Figure 1c and Table S1), including OS (*f*), electron transfer, HOMO/LUMO gap, D-index, MPI, and the minimal value of ESP. It should be noted that OS is the most relevant factor for fluorescence intensity, for which **1-MSA** was ranked as the largest with an *f* value of 0.1702 a.u., followed by an order of **1-MPA** ($f = 0.1648$ a.u.) > **1-ME** ($f = 0.1577$ a.u.) > **1-AM** ($f = 0.1575$ a.u.). It is also found that the electron transfer quantity is the only positively correlated one to OS, displaying an ascending order of **1-MSA** ($-1.9399\ e^-$) > **1-MPA** ($-1.0406\ e^-$) > **1-ME** ($-0.1032\ e^-$) > **1-AM** ($0.0009\ e^-$) and aligning well with the electron-transferring capability of the thiols in terms of their molecular configuration. The values of the HOMO/LUMO gap (4.6690–4.8560 eV) varied in a narrow range, implying the computation towards other quantities would be reliable under the same excitation conditions. Further hole–electron analysis of the S1→S0 emission shows that all the hole and the electron distributions (D index) did not separate obviously across the middle pentatomic and the left hexatomic ring with the D index ranging from 0.4630–1.5910 Å, which is approximately equal to the length of a C–C bond (≈1.45 Å). The four thiols substituted triatomic rings display the same outcome in terms of D index with the one before substituted by thiols (D index = 1.0390 Å), thus, it can be concluded that the D index is not the key factor to impact on the fluorescence emission. Moreover, neither the minimal value of ESP

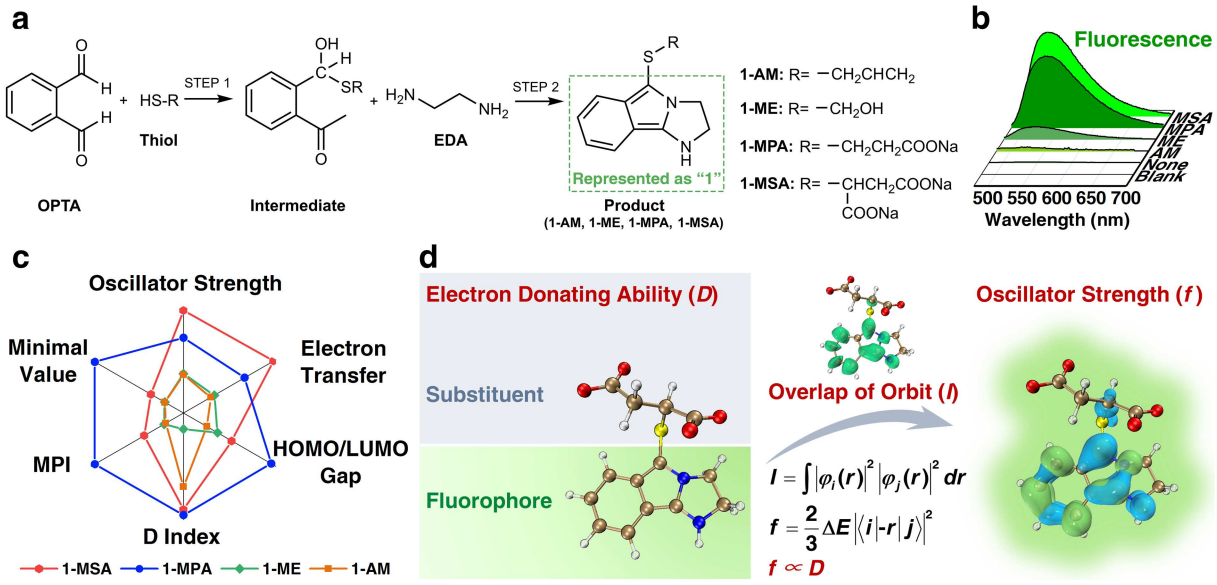

Figure 1. a) The proposed reaction mechanism of OPTA/thiol recognizing EDA and the structures for a set of thiols used in this work. b) The fluorescence spectra for the product from the reaction between OPTA and EDA in the presence of different thiols. c) The radar map for the main physical quantities of model molecules with different substituents. d) Schematic correlation between electron-donating capability, overlap of orbit and oscillator strength.

(−35.1986–−167.9244 kcal mol^{-1}) reflecting how HS–R affects the entire ESP of the triatomic ring nor the MPI (14.8286–73.9305 a.u.) depicting the interaction with the solvent fluctuate irregularly, being out of proportion with the tendency of OS and further suggesting a negligible role in the assessment.

Furthermore, it is appealing to specify how the electron-donating capability affects the OS. Thus, a correlation is found in equations [Eq. (1) and (2) in Figure 1d],[24] OS is determined by the transition dipole moment which is up to the orbital overlapping degree. Furthermore, to specify how the electron-donating capability affects OS, a correlation between OS and the orbital overlapping degree (I) was established through the transition dipole moment since it determines OS and is determined by the orbital overlapping degree. In view of the distortion of the tricyclic structure, it is found that a total value of bond angles of 347.795° in **1-MSA** is at least 3.318° more than the configurations of the other molecules, illustrating the electron-donating capability of the thiol in **1-MSA** effectively restrains the distortion and stabilizes the conjugation plane (Figure S2, Table S2). In addition, from the molecular orbital analysis of the specific excited state of the fluorescence-emission (S1→S0), it can be seen that I in **1-MSA** presented the largest value of 0.7572 and was followed by **1-MPA** (−0.6940), **1-ME** (−0.6692) and **1-AM** (0.5106), exhibiting a great agreement with the f value in order (Figure S3a). Therefore, it can be evidently concluded that a stronger electron-donating capability contributes to a more conjugated structure which allows a greater extent of orbital overlapping as well as a strengthened OS, finally leading to an elevated fluorescence emission. From the calculated fluorescence spectra (Figure S3b), it is shown that the fluorescence intensity from **1-MSA** is relatively higher than those of the others, while all emission spectral contours maintain similar patterns, in good agreement with the experimental results, confirming that the electron-donating ability does play a dominant role in determining the intensity of the fluorescence emission.

Colorimetric-Fluorescent Dual-Mode Sensing of EDA Solution

Experimentally, this electron-tuning strategy facilitating fluorescence enhancement would also bring about the changes in the ultraviolet-visible (UV/Vis) properties. The concentration-dependent investigation shows the sensing performances of the best combined reagents of OPTA and MSA (named as OPTA-MSA) towards EDA in the liquid phase with an evident colour trend from transparent to yellow with an increasing concentration of EDA from 0 to 30 μM under the optimized conditions (Figures 2a, S4). Considering that the colour visualization allows broader and more practical application, a naked-eye discrimination threshold was defined when the faint yellow starts to be distinguished by the naked-eye at an EDA concentration of 2 μM in colorimetric mode. Furthermore, as expected, the UV/Vis spectra showed a remarkable enhancement of the peak appearing at 468 nm after reacting with different concentrations of EDA (0–200 μM, Figure 2b). The correlation between the elevated absorption and the EDA concentration was further analyzed and the fitted curves show a great linearity in the range of 0–80 μM and a limit of detection (LOD) calculated as 42 nM (defined as LOD = $3\sigma/k$, where k is the slope of the linear part of the calibration curve (0.0363), and σ is the standard deviation of noise (0.5), Figure S5a). To confirm the specificity of OPTA-MSA toward the detection of EDA, the responses of 29 substances consisting of amines, water-soluble metallic salts,

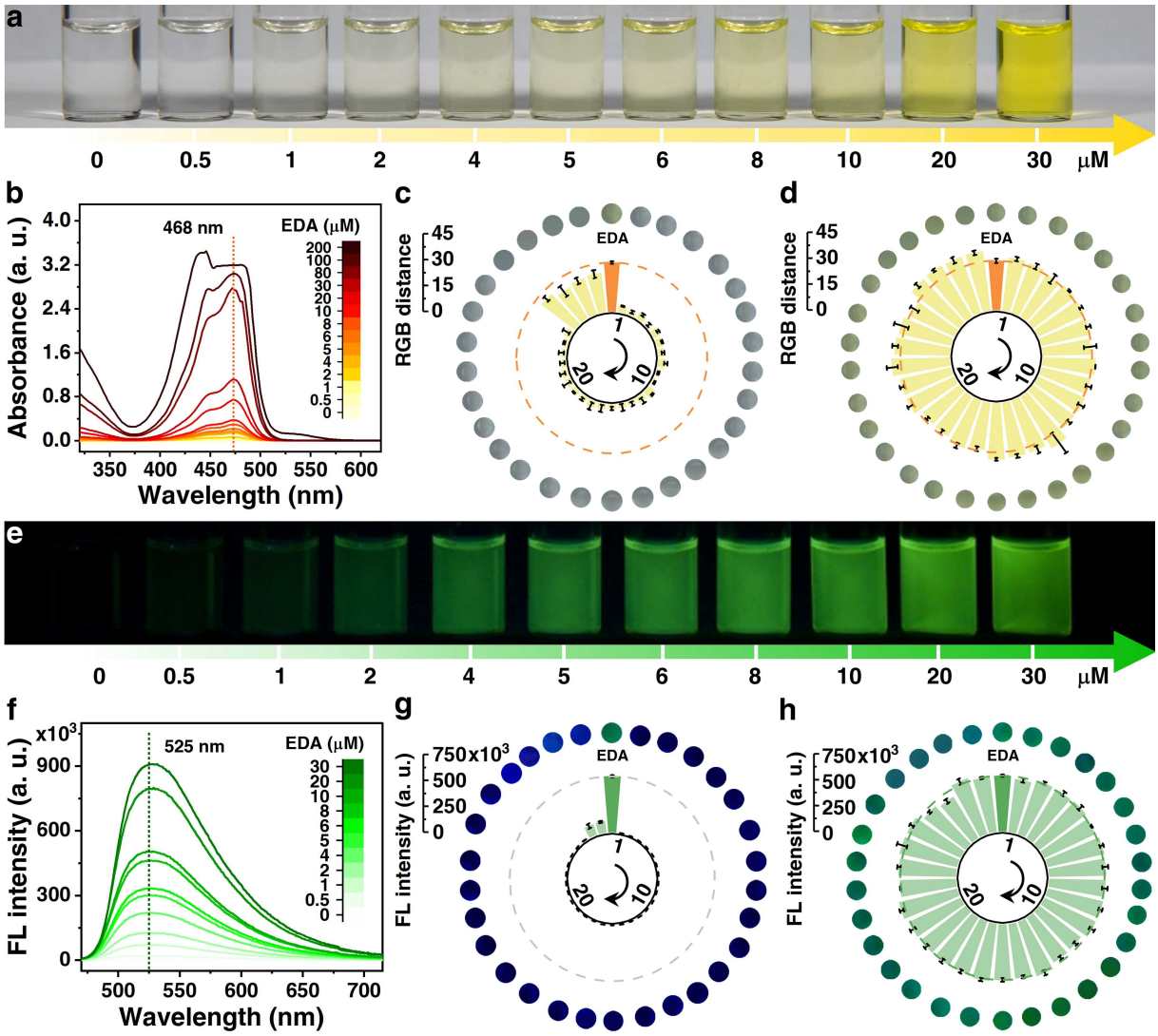

Figure 2. The optical images of the responses and spectra from OPTA-MSA towards EDA under a), b) colorimetric and e), f) fluorescent modes; c), g) the colorimetric RGB distance values and fluorescence (FL) intensities at 525 nm of the OPTA-MSA in response to EDA (0.02 μmol, sample 1), the potential co-existing substance and structural analogs (2 μmol, sample 1–29), respectively; d), h) the colorimetric RGB distance values and fluorescence intensities at 525 nm of the OPTA-MSA in response to the EDA solution (0.02 μmol, sample 1) and the mixtures of EDA (0.02 μmol) and the potential co-existing substance or structural analogs (2 μmol, sample 1–29). Note: the optical images in (a), (e) and the inserts in (c), (d), (g) and (h) were recorded under natural light (colorimetric mode) and an excitation of 468 nm (fluorescent mode). The error bars represent the relative standard deviations to the mean value ($n=3$).

hazardous chemicals, colored phosphors and daily compounds with 100 times higher concentration were compared with that of EDA. By analyzing the RGB distance of the samples before and after incubating with OPTA-MSA, 10 μM EDA resulted in an emerging yellow with an RGB distance of 28, while the other co-existing substances with higher concentration than EDA had no apparent colour change except the blue, the orange, the yellow and the green phosphors (Figure 2c). Consequently, the innate colour of these phosphors cannot be completely discriminated from EDA as the minimal difference in value is just around 14.77 %. It is further shown that the anti-interference capability of OPTA-MSA in response to EDA with the potential influence from the above-mentioned co-existing substances and structural analogues has imperceptible changes in the RGB distance in contrast to that of EDA only, with a deviation of the RGB distance which fluctuated less than 22.60 % (Figure 2d).

To further promote the sensing performances and get rid of the impact of colored substances, the intrinsic fluorescence behaviors of the reaction between OPTA, MSA and EDA were evaluated. A concentration-dependent green fluorescence enhancement with an increasing concentration of EDA from 0 to 30 μM was displayed and a pale-green with the minimal EDA concentration of 0.5 μM can be discerned by the naked-eye (Figure 2e). From the corresponding spectra (Figures 2f, S5b), it is shown that the fluorescent responses increased along with the EDA con-

centration ranging from 0.5 to 30 μM and a LOD of 0.17 nM can be obtained with a linear fitting in the range of 0–10 μM ($k = 54\,996$, $\sigma = 3$). Apparently, either the naked-eye detection threshold or the calculated LOD under the fluorescence mode are much superior than those of the above colorimetric mode as well as the previously reported fluorescence or colorimetry involved methods (Table S3). It is obvious this desirable response can be ascribed to the electron-donating capability dominated fluorescence emission which allows EDA to be probed even at an extremely low trace amount. From the evaluations of the specificity and the anti-interference capability (Figures 2g,h, Figure S6), only the four colored phosphors (interferents 26–29) showed blue fluorescence, and the emission peaks locate away from the response towards EDA at 525 nm, implying the inherent fluorescence of these colored phosphors can be discriminated from the recognition towards EDA. Furthermore, although the innate fluorescence of the existence of four phosphors slightly overlapped with the fluorescence response for EDA with a maximal influence of less than 15.4 %, the greenish turn-on fluorescence was not greatly changed in the presence of the above-mentioned interferents with 100 times higher concentration than that of EDA. Furthermore, the entire sensing process could be visualized within 2 s, starting from the addition of EDA to the appearance of a distinguishable green emission (Figure S7). This rapid response can be ascribed to the extraordinarily strong fluorescence from **1-MSA**, in which a relatively rigid plane guarantees less inactivation due to molecular vibration and intermolecular collision, further minimizing the outward energy transfer. Overall, these results reveal that both colorimetric and fluorescent modes provide good performances in sensing EDA, especially the fluorescence mode presents better sensitivity and the ability of distinguishing EDA with potential co-existing substances and analogues due to the successful modulation of the electron-donating capability of thiols. Meanwhile, the visualized observation under the colorimetric mode contributes more practicability at a certain concentration range, the combined dual-mode sensing strategy would enable a more accurate and reliable detection owing to the synergic and complementary responses.

To realize portable EDA detection, the paper-based sensing chip was fabricated by embedding OPTA-MSA into the filter paper. Upon the responses towards the incremental EDA solution, the paper-based sensing chip exhibited a naked-eye enabled LOD of 5 μM for the dual-mode detection (Figures S8, S9). To further evaluate the sensing performances for real sample analysis, EDA was spiked in the effluent collected from a local sewage treatment plant (STP) to introduce more uncertainty from the potential co-existing interferents. The sensing results show a great alignment with the responses in the detection under the laboratory conditions. With the analysis of the chromatic aberration (ΔE) in CIELab color space[25] from the responses of the paper-based sensing chip towards EDA solution, it can be easily concluded that the LOD by the naked eye under colorimetric and fluorescent modes are 10 μM and 5 μM. This result confirms a higher sensitivity of the fluorescent mode which is lower than the threshold level of EDA (0.5 mg L^{-1}, equal to 8.3 μM) in effluent from STP specified by the European Union,[26] illustrating the superior detection capability of the paper-based sensing chip for potential industrial applications.

Hydrogel-Based Sensing Chip-Enabled Dual-Mode Detection of EDA Vapor

Considering that monitoring on EDA vapor is of great significance to screen spillage events or terrorist activity, a hydrogel-based gaseous sensing platform with dual-mode response was constructed by adopting the chemically cross-linked polyvinyl alcohol (PVA) hydrogel as the support to immobilize the OPTA-MSA reagent (Figure 3a). It should be noted that the three-dimensional porous network structure is inert to OPTA-MSA, benefiting the observation of the intrinsic dual-mode sensing signal (Figure S10). It is obvious that a color change from off-white to yellow and a green fluorescence lighting were observed due to the effective adsorption and specific identification of the OPTA-MSA loaded hydrogel substrate towards EDA molecules when the hydrogel-based sensing chip was exposed to EDA vapor. Under an exposure duration of 90 s in EDA with a concentration of 3.2 to 160 ppm, both the colorimetric and fluorescent channels reached the most distinct coloring at 64 ppm and remained unchanged along with the further increased EDA concentration (Figure 3b). This saturation trend could be sufficiently described by the numerical analysis based on the RGB value extraction. The stepwise increase from 3.2 ppm to 48 ppm with a linear relationship was followed by a sharp rise and then the value reached a plateau from 64 ppm to 160 ppm under the colorimetric channel (Figure 3c). While a wider linear range from 3.2 to 64 ppm was achieved under the fluorescent mode with a more gradual increase until reaching the saturated status after 64 ppm, and the whole tendency shows smaller data deviations (Figure 3d). This comparison indicates that both modes possess the quantification capability from several to dozens of ppm level and the fluorescence mode is more adoptable for quantitative analysis due to a wider linear relationship between the amount of EDA and the sensing signal.

Furthermore, an ascending trend was displayed and a linearly fitted correlation between ΔE in CIELab color space and concentration was fulfilled under both modes. As the ΔE under these two modes were 5.5 and 4.9 in detecting 3.2 ppm EDA vapor (Figure 3e), implying an accessible identification by the naked eye and an adequate detection limit which is lower than the exposure limit of 25 mg m^{-3} (equal to10 ppm) EDA vapor stated by the WHO.[3] In particular, under the fluorescent mode, when ΔE is equal to 1, which is considered to be discriminable by the naked eye,[27] the calculated concentration of EDA vapor is 700 ppb, indicating that the hydrogel-based sensing chip could realize a ppb level response. It is undoubtable that the intrinsically superior detection capability of OPTA-MSA towards EDA, the good distribution of the sensing reagent

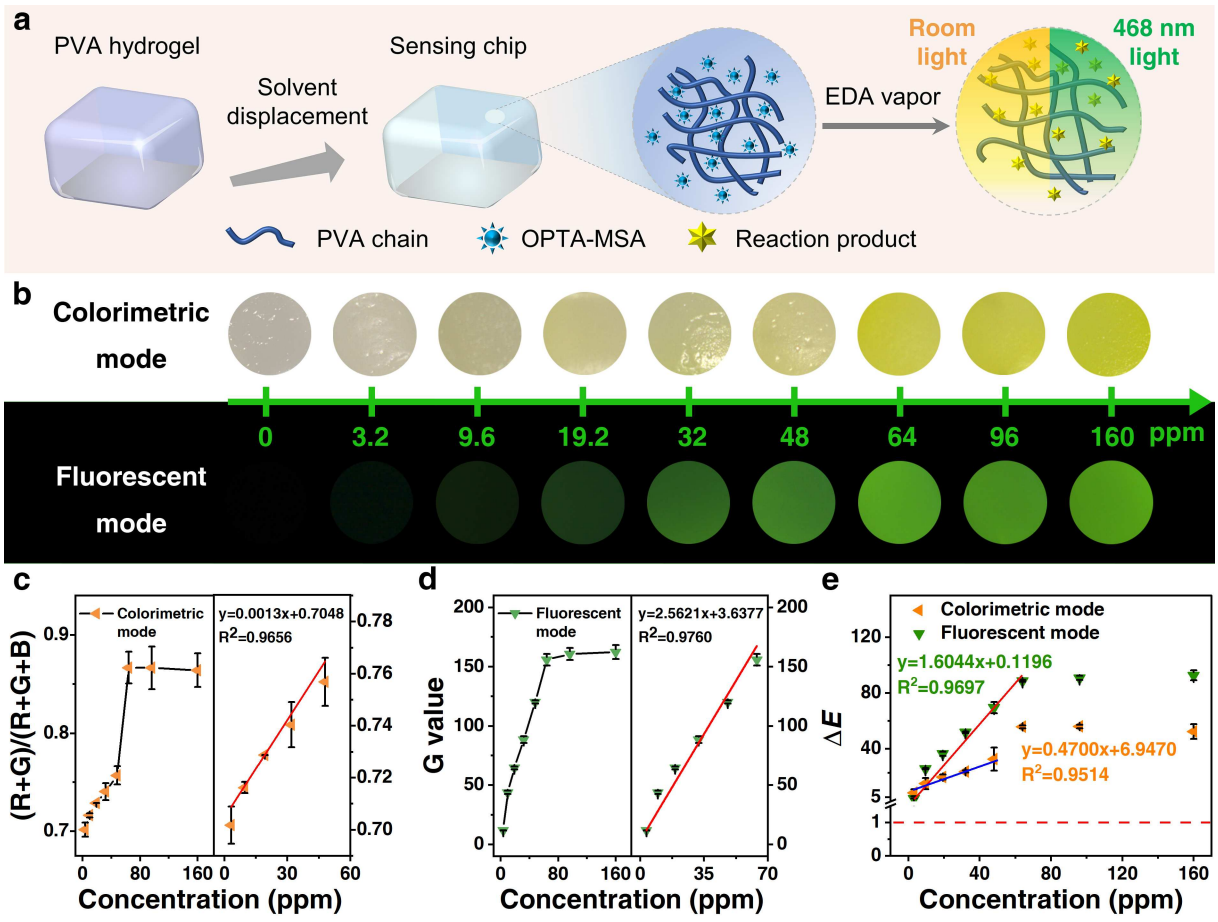

Figure 3. a) Construction of the OPTA-MSA loaded PVA hydrogel-based sensing chip for EDA vapor detection. b) The colorimetric and fluorescent images of detecting EDA vapor with a series of concentrations; the plotting curves of c) (R+G)/(R+G+B) value and d) G value extracted from the dual-mode hydrogel-based sensing chip versus the EDA concentration, and e) the corresponding relations between ΔE of the color/fluorescence responses of the hydrogel-based sensing chip versus EDA vapor with different concentrations.

enabled homogeneous response, as well as the effective confinement of the three-dimensional porous network structure together facilitate the PVA hydrogel-based sensing chip a prominent application in probing trace levels of EDA vapor.

Additionally, from the investigation of the specificity of the hydrogel-based sensing platform towards EDA vapor and the atmosphere of common volatile substances, organic solvents in laboratory and daily products, only the emergence of EDA vapor can cause the change in colour from light grey to bright yellow and produce green fluorescence (Figure S11). It should be noted that other interferents can only result in a non-characteristic colour change and cannot give rise to any fluorescence emission. Thus, the hydrogel-based dual-mode sensing results demonstrated that the interferential vapors have no influence on the EDA analysis and it is of great potential to be used in complicated sensing environments.

Portable Detector Enabled On-Site EDA Vapor Monitoring

Considering the limited discernibility of the human eye for subtle color changes and to further reinforce the detection reliability and the operation integration, the dual-mode PVA hydrogel-based sensing chip was integrated into a sensing array of a homemade portable detector (Figure 4a). In routine operation, the unknown atmosphere was inhaled into the detector via a pumping system, with which the gaseous molecules or particulates in the airstream could fall onto the sensing chip with the help of a holder. Any change of the sensing chip in color could be recorded by the integrated optical system, and the recorded photograph was then analyzed via a data processing module followed by a delivery of the outcome to the liquid crystal display (LCD) screen and the cloud platform. The Yes/No answer was generated via the decision-making logic based on the dual-mode sensing result (Figure 4b), thus, it is expected that once EDA concentration in a specific area reaches the threshold value, the warning reminder is triggered and the corresponding warning information could be instantaneously displayed and uploaded.

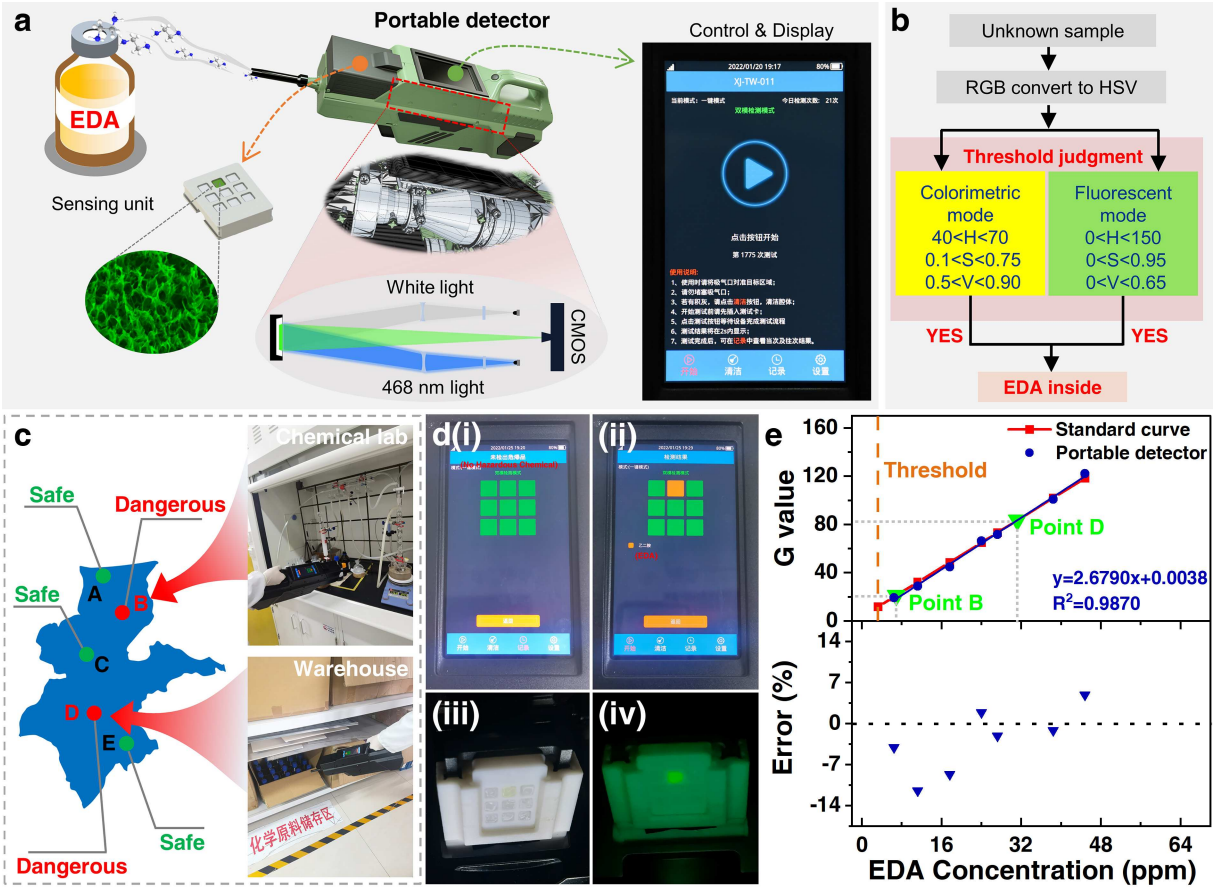

Figure 4. a) Schematic illustration of the portable detector for on-site EDA vapor measurement. b) Flow chart of the decision-making logic. c) Schematic diagram of the EDA detection in the simulation scenes. d) The images of the display screen shown in i) safe and ii) warning, the images of the sensing array for the measurement at site B shown under iii) white light and iv) 468 nm illumination. e) The calibration curve (top, blue) built through the portable detector pumping sampling compared with the responses of the hydrogel sensing chip (top, red) towards the standard EDA vapor, and the corresponding errors (bottom).

In specific scenarios, the portable detector was employed to examine the atmosphere in a series of locations (sites A to E), including factory (A, C, and E), chemical lab (B) and warehouse (D), where relatively high risk of EDA spillage exists (Figure 4c). Based on the dual-mode judgment of the detector, the EDA concentrations at sites A, C and E lower than the threshold value (3.2 ppm) were shown in green at the second grid of the first row (2nd cell of 1st row) and a Chinese phrase reminder standing for "No Hazardous Chemical" (Figure 4d (i)), suggesting safe; while those at sites B and D exceeded the threshold value and were displayed in orange as well as the Chinese word representing "EDA" (Figure 4d (ii)), warning the high risk of an EDA spillage event. Subsequently, the sensing array in the measurements of sites B and D was taken out, in which the 2nd cell of the 1st row exhibited yellow (Figure 4d (iii)) and green fluorescence (Figure 4d (iv)) under a dual-mode light source, illustrating the same sensing responses towards EDA vapor as the hydrogel sensing chip did. These EDA sensing cells (2nd cell of 1st row) were processed with the same procedure as the hydrogel sensing chip, the corresponding concentrations at sites B (6.9 ppm) and D (31.2 ppm) were obtained through the semi-quantitation based on the calibration curve, in which each datum was generated with the same pumping sampling, and its linearity aligned well with the fluorescent responses of the standard EDA concentrations with the error restrained within 11.4 % (Figure 4e). This illustrates that the functional integration of the semi-quantitation would be feasible and indispensable for updating the portable detector. Besides, the total on-site detection time was around 16 s (Supporting Information Video), including the entire running process starting with pumping sampling, detection with the hydrogel chip, data process and ending with the outcome output, which was fast enough to meet the on-site application requirements. Therefore, it is clearly indicated that the sensing performance of the present portable detector is reasonably reliable to play a substantial role in online, real-time monitoring of a potential leakage without extra manpower, no matter for EDA or other risky gases.

Conclusion

In summary, in this work a fundamental investigation regarding the essence of how physical quantities act on fluorescence behavior was conducted by constructing a thiol-mediating imidazo isoindole fluorophore as the modal molecule, which was further employed to ultrasensitively detect trace EDA. By thoroughly analyzing the individual influence as well as the interplay between multi-descriptor, the finely modulated electron-donating capability of thiol was proven as the prominent descriptor corelating to the fluorescence intensity. Consequently, MSA with remarkable electron-donating capability was verified to give rise to an intense fluorescence. Experimental demonstration empowered a quantitative detection of EDA, accompanied by a dual-response composed of a color change and a turn-on green fluorescence. The excellent sensing performances including ultrahigh sensitivity, outstanding selectivity and anti-interference capability facilitated a desirable analysis of EDA in industrial wastewater. Expanding on this preliminary trial, the proposed sensing reagent loaded hydrogel substrate was assembled in a portable detector which gathered the merits of rapid response, automation, as well as on-site detection, it was further proven to be practicable and reliable in real environmental applications. We conjecture the insight gained regarding the electron transferring predominated fluorescence model would become a representative example in guiding customizable optical molecules from wider perspectives, thereby accelerating practical application in relevant fields of sensing, imaging, catalysis as well as solar cell, etc.

Acknowledgements

We gratefully acknowledge financial support from the Natural Science Foundation of Xinjiang (2021D01D04), National Natural Science Foundation of China (21974150, U1903306), the Youth Innovation Promotion Association, CAS (No. 2018474), West Light Foundation of the Chinese Academy of Sciences (CAS Grant No. 2020-XBQNXZ-022), Key Research Program of Frontier Sciences (CAS Grant No. ZDBS-LY-JSC029), and the technical support from the open-source software Multiwfn: A Multifunctional Wavefunction Analyzer.

Conflict of Interest

The authors declare no conflict of interest.

Data Availability Statement

The data that support the findings of this study are available from the corresponding author upon reasonable request.

Keywords: Ethylenediamine · Explosives · Fluorescence · Trace Sensing · Ultrasensitive Detection

[1] a) S. Freddi, M. C. R. Gonzalez, P. Carro, L. Sangaletti, S. De Feyter, *Angew. Chem. Int. Ed.* **2022**, *61*, e202200115; *Angew. Chem.* **2022**, *134*, e202200115; b) G. Wang, Y. Li, Z. Cai, X. Dou, *Adv. Mater.* **2020**, *32*, 1907043; c) K. C. To, S. Ben-Jaber, I. P. Parkin, *ACS Nano* **2020**, *14*, 10804; d) J. Y. Lee, H. D. Root, R. Ali, W. An, V. M. Lynch, S. Bahring, I. S. Kim, J. L. Sessler, J. S. Park, *J. Am. Chem. Soc.* **2020**, *142*, 19579.

[2] a) B. Wu, Z. Zhou, F. Li, L. Yang, T. Zhang, J. Zhang, *New J. Chem.* **2013**, *37*, 646; b) J. Burrows, S. Kamo, K. Koide, *Science* **2021**, *374*, 741; c) Y. Xie, P. Hu, Y. Ben-David, D. Milstein, *Angew. Chem. Int. Ed.* **2019**, *58*, 5105; *Angew. Chem.* **2019**, *131*, 5159; d) X. Liu, W. Ma, X. Lei, S. Zhang, Y. Ding, *Adv. Funct. Mater.* **2020**, *30*, 2002120.

[3] R. Cary, S. Dobson, J. Delic, *1,2-Diaminoethane, ethylenediamine*, World Health Organization, Geneva, **1999**.

[4] H. Maurer, K. Pfleger, *Fresenius Z. Anal. Chem.* **1988**, *331*, 744.

[5] K. Andersson, C. Hallgren, J. O. Levin, C. A. Nilsson, *Am. Ind. Hyg. Assoc. J.* **1985**, *46*, 225.

[6] X. Zhang, K. Li, H. Li, J. Lu, Q. Fu, Y. Jia, W. Li, *J. Mater. Sci.* **2015**, *50*, 4288.

[7] Y. J. Jin, G. Kwak, *Sens. Actuators B* **2018**, *271*, 183.

[8] Y. Kim, S. H. Son, T. S. Lee, *Mol. Cryst.* **2014**, *600*, 179.

[9] a) J. Wang, D. Li, Y. Ye, Y. Qiu, J. Liu, L. Huang, B. Liang, B. Chen, *Adv. Mater.* **2021**, *33*, 2008020; b) T. Liu, W. Wang, D. Jian, J. Li, H. Ding, D. Yi, F. Liu, S. Wang, *Sens. Actuators B* **2019**, *301*, 127168; c) D. Laskaratou, G. S. Fernandez, Q. Coucke, E. Fron, S. Rocha, J. Hofkens, J. Hendrix, H. Mizuno, *Nat. Commun.* **2021**, *12*, 2541; d) K. Liu, C. Shang, Z. Wang, Y. Qi, R. Miao, K. Liu, T. Liu, Y. Fang, *Nat. Commun.* **2018**, *9*, 1695.

[10] a) P. Li, D. Yang, H. Li, *Dyes Pigm.* **2016**, *132*, 306; b) Y. Xu, S. Yu, Q. Chen, X. Chen, Y. Li, X. Yu, L. Pu, *Chem. Eur. J.* **2016**, *22*, 12061; c) Y. Xu, S. Yu, Y. Wang, L. Hu, F. Zhao, X. Chen, Y. Li, X. Yu, L. Pu, *Eur. J. Inorg. Chem.* **2016**, 5868; d) S. B. Seenivasagaperumal, S. Shanmugam, *New J. Chem.* **2018**, *42*, 3394; e) M. Saravanakumar, B. Umamahesh, R. Selvakumar, J. Dhanapal, S. K. Ashokkumar, K. I. Sathiyanarayanan, *Dyes Pigm.* **2020**, *178*, 108346.

[11] a) D. Denkova, M. Ploschner, M. Das, L. M. Parker, X. Zheng, Y. Lu, A. Orth, N. H. Packer, J. A. Piper, *Nat. Commun.* **2019**, *10*, 3695; b) I. H. Cho, L. Mauer, J. Irudayaraj, *Biosens. Bioelectron.* **2014**, *57*, 143; c) Y. Lu, J. Zhao, R. Zhang, Y. Liu, D. Liu, E. M. Goldys, X. Yang, P. Xi, A. Sunna, J. Lu, Y. Shi, R. C. Leif, Y. Huo, J. Shen, J. A. Piper, J. P. Robinson, D. Jin, *Nat. Photonics* **2014**, *8*, 32.

[12] L. Wu, C. Huang, B. P. Emery, A. C. Sedgwick, S. D. Bull, X. P. He, H. Tian, J. Yoon, J. L. Sessler, T. D. James, *Chem. Soc. Rev.* **2020**, *49*, 5110.

[13] a) N. Kaur, P. Alreja, *J. Chem. Sci.* **2015**, *127*, 1253; b) N. Bian, Q. Chen, X. L. Qiu, A. D. Qi, B. H. Han, *New J. Chem.* **2011**, *35*, 1667.

[14] L. Yang, M. Wang, P. M. Slattum, B. R. Bunes, Y. Wang, C. Wang, L. Zang, *ACS Appl. Mater. Interfaces* **2018**, *10*, 19764.

[15] Y. H. Chen, R. Sung, K. Sung, *Phys. Chem. Chem. Phys.* **2020**, *22*, 2424.

[16] A. Hussain, H. Yuan, W. Li, J. Zhang, *J. Mater. Chem. C* **2019**, *7*, 6685.

[17] a) B. Jędrzejewska, P. Krawczyk, M. ózefowicz, *Spectrochim. Acta Part A* **2017**, *171*, 258; b) M. Khadem Sadigh, M. S. Zakerhamidi, *Spectrochim. Acta Part A* **2020**, *239*, 118445.

[18] J. S. Murray, P. Politzer, *Electrostatic potentials: chemical applications*, Wiley, Hoboken, **2002** (https://doi.org/10.1002/0470845015.cca014).
[19] Y. Gao, X. D. Yang, S. X. Wu, Y. Geng, *Adv. Theory Simul.* **2019**, *2*, 1900076.
[20] H. Kim, W. Park, Y. Kim, M. Filatov, C. H. Choi, D. Lee, *Nat. Commun.* **2021**, *12*, 5409.
[21] J. S. Jang, H. L. Lee, K. H. Lee, J. Y. Lee, *J. Mater. Chem. C* **2019**, *7*, 12695.
[22] a) B. D. Wagner, G. J. McManus, *Anal. Biochem.* **2003**, *317*, 233; b) P. Zuman, *Chem. Rev.* **2004**, *104*, 3217.
[23] a) S. A. Berhe, M. T. Rodriguez, E. Park, V. N. Nesterov, H. Pan, W. J. Youngblood, *Inorg. Chem.* **2014**, *53*, 2346; b) T. Otsuka, M. Sumita, H. Izawa, K. Morihashi, *Phys. Chem. Chem. Phys.* **2018**, *20*, 3911.
[24] a) I. N. Levine, *Quantum Chemistry*, 7th ed., Pearson Education, New York, **2014**; b) T. Lu, F. W. Chen, *J. Comput. Chem.* **2012**, *33*, 580.
[25] a) J. Schanda, *Colorimetry: understanding the CIESystem*, Wiley, Hoboken, **2007**; b) S. Lathwal, H. D. Sikes, *Lab Chip* **2016**, *16*, 1374.
[26] C. European, in *Official Journal of the European Union*, **2006**, pp. 1–849.
[27] M. M. Hawkeye, M. J. Brett, *Adv. Funct. Mater.* **2011**, *21*, 3652.

Manuscript received: March 3, 2022
Accepted manuscript online: April 1, 2022
Version of record online: ■■, ■■

Forschungsartikel

Organic Sensors

Y. Ke, Y. Liu, B. Zu,* D. Lei, G. Wang, J. Li, W. Ren, X. Dou* **e202203358**

Electronic Tuning in Reaction-Based Fluorescent Sensing for Instantaneous and Ultrasensitive Visualization of Ethylenediamine

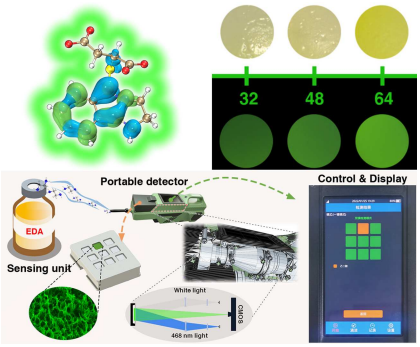

A positive correlation was built between the electron-donating capability and fluorescence intensity based on a molecular mode of how physical quantities affect optical behavior. This model has a fluorescent-colorimetric dual-response with nanomolar-liquid/ppb-vapor ultrasensitivity to ethylenediamine (EDA), which was integrated into a gas detector, fulfilling real-time management of EDA to address leakage risk and threat to public safety.